



**HAL**  
open science

# Multi-parameter multiplicative regularization: an application to force reconstruction problems

Mathieu Aucejo, Olivier de Smet

► **To cite this version:**

Mathieu Aucejo, Olivier de Smet. Multi-parameter multiplicative regularization: an application to force reconstruction problems. *Journal of Sound and Vibration*, 2020, 469, pp.115135. 10.1016/j.jsv.2019.115135 . hal-02424030

**HAL Id: hal-02424030**

**<https://hal.science/hal-02424030>**

Submitted on 26 Dec 2019

**HAL** is a multi-disciplinary open access archive for the deposit and dissemination of scientific research documents, whether they are published or not. The documents may come from teaching and research institutions in France or abroad, or from public or private research centers.

L'archive ouverte pluridisciplinaire **HAL**, est destinée au dépôt et à la diffusion de documents scientifiques de niveau recherche, publiés ou non, émanant des établissements d'enseignement et de recherche français ou étrangers, des laboratoires publics ou privés.

# Multi-parameter multiplicative regularization: an application to force reconstruction problems

M. Aucejo<sup>a</sup>, O. De Smet<sup>a</sup>

<sup>a</sup>*Structural Mechanics and Coupled Systems Laboratory, Conservatoire National des Arts et Métiers, 2 Rue Conté, 75003 Paris, France*

---

## Abstract

This paper introduces a multi-parameter multiplicative regularization for force reconstruction problems. This approach allows exploiting the local prior information available on the sources to identify, while determining the related regularization parameters in an elegant and efficient manner. The aim of this paper is to assess the applicability of a multi-parameter regularization strategy compared to a single parameter formulation for reconstructing the external sources acting on a mechanical structure. A particular attention is also paid to the practical resolution of the regularization problem by implementing an original Iteratively Reweighted algorithm derived from the direct application of the first-order optimality condition. The performance of the proposed algorithm in terms of solution accuracy is compared with a more classical implementation based on an Iteratively Reweighted Least-Squares procedure. The interest of the proposed multi-parameter strategy is assessed numerically. Obtained results demonstrates that consistent reconstructions are obtained for high and moderate measurement noise level whatever the formulation considered (i.e. single or multi-parameter) provided that the

---

\*Corresponding author. E-mail address: mathieu.aucejo@lecnam.net

suitable resolution algorithm is implemented. For very and extremely noisy input data, the single parameter strategy is more robust than the multi-parameter approach.

*Keywords:* Linear inverse problem, Force reconstruction, Multi-parameter multiplicative regularization, Iteratively Reweighted algorithm.

---

## 1. Introduction

For solving force reconstruction problems, additive regularizations are commonly implemented. Among all this class of methods, the most popular technique is certainly the Tikhonov regularization, a.k.a.  $\ell_2$ -regularization [1–6]. It should however be noted that this approach generally promotes smooth solutions [7, 8], which generally leads to qualitatively poor reconstructions when the excitation field or the excitation signal is rather sparse. In the latter situation, the LASSO regularization, a.k.a.  $\ell_1$ -regularization, has been proposed to enforce the sparsity of the regularized solutions [9–12]. In the context of force reconstruction, these approaches have been unified and generalized by Aucejo through the introduction of the  $\ell_q$ -regularization, which allows the resolution of non-convex sparse minimization problems [13]. However, all the above-mentioned procedures assumes a global a priori on the sources to identify. Incidentally, poor reconstructions can be obtained in situations where a structure is excited by several sources having different spatial distributions. From a theoretical standpoint, the corresponding regularization term, encoding all the prior information on the sources to identify, is not perfectly adapted to properly reflect the actual distribution of each source. To overcome this weakness, Aucejo and De Smet have sought

to exploit any local prior information available by defining several identification regions, for which a local  $\ell_q$ -regularization term is employed [14]. Despite their efficiency for solving force reconstruction problems, all these additive regularization techniques requires a proper tuning of the regularization parameter appearing in their mathematical formulation. Because this task proves to be difficult in practice, a multiplicative  $\ell_q$ -regularization has been recently introduced for reconstructing mechanical sources [15]. Initially developed by Van den Berg et al. [16], this regularization technique consists in including the regularization term as a multiplicative constraint in the formulation of the inverse problem. The main advantage of this regularization strategy is to avoid the preliminary definition of any optimal regularization parameter, since it is defined and computed during the resolution process. In Ref. [15], the proposed multiplicative regularization, called ordinary multiplicative regularization (OMR) in the rest of this paper, is established by assuming that the structure is excited in different regions by local excitation fields of various types. In the latter contribution, the regularization term is defined as the sum of local regularization terms, encoding available prior information on the excitation field to identify in each region.

A potential drawback of the above-mentioned strategy is the definition of a single regularization parameter for all the regions considered. A thorough analysis of the existing literature indeed suggests that, when the solution to identify exhibits several distinct features simultaneously, multi-parameter additive regularization may perform better than a single parameter regularization parameter, because each individual feature can be emphasized through the definition of a corresponding regularization parameter [17–24]. Despite

these encouraging results, one of the main challenges is the selection of suitable regularization parameters. In this regard, several approaches have been proposed. Generally, they are a generalization of the corresponding one parameter procedure, such as the L-hypersurface [25], the multivariate GCV [26], the generalized discrepancy principle [27, 28] or the generalized Regińska criterion [29].

Based on this extensive literature, it seems legitimate to develop a multi-parameter regularization strategy for force reconstruction problem, combining the advantages of a multi-parameter formulation and the multiplicative regularization. This idea, which is at the core of the present paper, gives rise to a particular form of the multiplicative regularization, named multi-parameter multiplicative regularization (MPMR) in the rest of the paper. This formulation is based on the work of Bazàn et al., suggesting that the regularization term can be expressed as the product of the local regularization terms [29].

The basic motivation of this paper is to assess the applicability and the performances of the MPMR for identifying mechanical sources in the frequency domain compared to the OMR previously proposed by the authors in Ref. [15]. To this end, the paper is divided into three parts. In section 2, the mathematical formulations of the OMR and the MPMR are presented to clearly highlight the main differences between both regularization strategies. Section 3 is dedicated to the description of the algorithms used to solve each formulation. More specifically, an original Iteratively Reweighted algorithm is derived for each of them from the direct application of the first-order optimality condition. This approach differs from the standard approach con-

sisting in implementing IRLS<sup>1</sup>-like algorithms, in which the considered regularization term is recast into a weighted  $\ell_2$ -regularization term. Finally, the applicability of the proposed multi-parameter approach for consistently reconstructing mechanical sources is illustrated numerically in section 4 by comparison with the related single parameter strategy. In particular, obtained results reveals that the OMR is more robust than the MPMR with respect to the measurement noise level, while the comparisons of the implementations of both formulation indicate that the proposed resolution algorithms perform better than the related IRLS versions in terms of solution accuracy.

## 2. Formulation of the ordinary and multi-parameter multiplicative regularizations

From a very general standpoint, the multiplicative regularization is mathematically expressed as:

$$\hat{\mathbf{F}} = \underset{\mathbf{F} \setminus \{0\}}{\operatorname{argmin}} \mathcal{F}(\mathbf{X} - \mathbf{H}\mathbf{F}) \cdot \mathcal{R}(\mathbf{F}), \quad (1)$$

where:

- $\mathcal{F}(\mathbf{X} - \mathbf{H}\mathbf{F})$  is the data-fidelity term controlling the a priori on the noise corrupting the data [30–32]. The argument of the data-fidelity term assumes a linear reconstruction model defined such that:

$$\mathbf{X} = \mathbf{H}\mathbf{F}, \quad (2)$$

---

<sup>1</sup>Iteratively Reweighted Least-Squares.

where  $\mathbf{X}$  is the vibration field,  $\mathbf{F}$  is the excitation field, while  $\mathbf{H}$  is the transfer functions matrix of the structure.

- $\mathcal{R}(\mathbf{F})$  is the regularization term encoding any prior information on the excitation field  $\mathbf{F}$  [33–35].

The previous relation clearly indicates that the quality of the reconstructed excitation field is strongly influence by the choice data-fidelity and regularization terms, which have to reflect the actual noise and the actual source characteristics. In this respect, the definition of the data-fidelity term classically assumes that the vibration field  $\mathbf{X}$  is corrupted by an additive Gaussian white noise. It results that the data-fidelity term can be expressed as [36–38]:

$$\mathcal{F}(\mathbf{X} - \mathbf{H}\mathbf{F}) = \|\mathbf{X} - \mathbf{H}\mathbf{F}\|_2^2. \quad (3)$$

The definition of the regularization term is less obvious and requires more attention, since it has to reflect the a priori experimenter’s knowledge of the sources to identify. Generally, forces of different nature and locations can act simultaneously on a structure. This is for this particular reason that it is supposed that the structure is excited in  $R$  different regions by local excitation fields  $\mathbf{F}_r$  of various types (localized or distributed, for instance). Formally, this naturally leads to introduced local regularization terms  $\mathcal{R}(\mathbf{F}_r)$ , which are defined such that [14, 15]:

$$\mathcal{R}(\mathbf{F}_r) = \|\mathbf{F}_r\|_{q_r}^{q_r}, \quad (4)$$

where  $q_r$  is the norm parameter defined on  $\mathbb{R}^{+*}$ ,  $\|\bullet\|_{q_r}$  is the  $\ell_{q_r}$ -norm or

quasi-norm.

Practically, there are two ways of combining these local regularization terms to form the regularization term  $\mathcal{R}(\mathbf{F})$ . The first one consists in defining the regularization term as the sum of the local regularization terms. This regularization term, derived from the Bayesian framework [14], is at the root of the ordinary multiplicative regularization (OMR) introduced in Ref. [15], namely:

$$\hat{\mathbf{F}} = \underset{\mathbf{F} \setminus \{0\}}{\operatorname{argmin}} \|\mathbf{X} - \mathbf{H}\mathbf{F}\|_2^2 \cdot \sum_{r=1}^R \|\mathbf{F}_r\|_{q_r}^{q_r}. \quad (5)$$

The second possibility consists in considering the regularization term as the product of the local regularization terms, as suggested by Bazàn et al. in Ref. [29]. Such a formulation gives rise to the multi-parameter multiplicative regularization (MPMR), defined such that:

$$\hat{\mathbf{F}} = \underset{\mathbf{F} \setminus \{0\}}{\operatorname{argmin}} \|\mathbf{X} - \mathbf{H}\mathbf{F}\|_2^2 \cdot \prod_{r=1}^R \|\mathbf{F}_r\|_{q_r}^{q_r}. \quad (6)$$

It is clear, from Eqs. (5) and (6), that the OMR and the MPMR reduce to the same regularization problem when only one identification region is defined. Actually, the main noticeable difference between both formulations appears when several identification regions are considered. In this situation, the definition of the adaptive regularization parameter<sup>2</sup>  $\alpha$  associated to each resolution algorithm differs. As it will be made clearer in the next section, the resolution of the OMR leads to the definition of a unique adaptive reg-

---

<sup>2</sup>This name has been given because the value of the regularization parameter of the multiplicative regularization is automatically adapted throughout the iterative process.

ularization parameter for all the considered identification regions, while the MPMR leads to the definition of  $R$  adaptive regularization parameters, i.e. one per identification region. Consequently, the MPMR has more degrees of freedom than the OMR for solving the inverse problem, which is potentially beneficial in terms of solution accuracy. These specificities are at the origin of the present contribution and their implications will be carefully analyzed in section 4.

### 3. Resolution algorithms

By construction, the resolution of the OMR and the MPMR requires the implementation of an iterative procedure. In general, an adapted IRLS algorithm is implemented for this purpose. In the present paper, we propose a novel Iteratively Reweighted (IR) algorithm for each formulation by directly applying the first-order optimality condition. In the rest of the paper, these algorithms will be respectively referred to as OMR-IR and MPMR-IR algorithms. Schematically, whatever the algorithm considered, the resolution process is divided into three main steps:

1. Set  $k = 0$  and initialize  $\widehat{\mathbf{F}}^{(0)}$
2. **while** convergence is not reached
  - a. Main iteration - Compute  $\widehat{\mathbf{F}}^{(k+1)}$
  - b. Monitor the convergence
- end while**
3. **return**  $\widehat{\mathbf{F}}$

To help the reader to have a global overview of the resolution process, each step of the proposed IR algorithms is introduced in a chronological order.

### 3.1. Initialization of the resolution algorithms

The definition of the initial solution can be one of the keys of the convergence of the proposed iterative procedures, especially when the functional to minimize is non-convex<sup>3</sup>. From our previous works, it has been shown that the solution of the standard Tikhonov regularization [13–15, 38–40] provides a reasonable initial solution to allow the convergence of the iterative process to a mechanically consistent reconstruction. Mathematically, the initial solution is consequently computed from the following equation:

$$\widehat{\mathbf{F}}^{(0)} = (\mathbf{H}^H \mathbf{H} + \alpha^{(0)} \mathbf{I})^{-1} \mathbf{H}^H \mathbf{X}, \quad (7)$$

where  $\mathbf{I}$  is the identity matrix, while  $\alpha^{(0)}$  is the initial adaptive regularization parameter.

The order of magnitude of the optimal regularization parameter being unknown from the data only, a rough estimate of  $\alpha^{(0)}$  is practically hard to define a priori, without using any selection procedures or large computational efforts. The only thing we know is that its value is generally set in the interval defined between the smallest and the largest singular values of  $\mathbf{H}$  [41]. To bypass this difficulty and preserve the advantage of the multiplicative strategy in terms of computational efficiency, some heuristics can be used.

---

<sup>3</sup>This situation arises for any  $q_r < 1$ .

In the present paper, we propose to apply the heuristic procedure introduced in Ref. [15]. Because this estimation procedure is heuristic, it may however fail to give a good starting point for the iterative process. In such a situation,  $\alpha^{(0)}$  can be selected using one of the automatic selection procedures available in the literature [42–45]. It should however be noted that the suitability of the value of  $\alpha^{(0)}$  (and that of  $\widehat{\mathbf{F}}^{(0)}$  by extension) can only be judged from the excitation field finally identified, that can be analyzed from the experimenter’s knowledge and any available prior information on the sources to identify<sup>4</sup>.

### 3.2. Main iteration

The main iteration consists in computing the solution at iteration  $k+1$  of the resolution process from the knowledge of the solution at the previous iteration of the algorithm.

#### 3.2.1. Main iteration for the OMR

For the OMR, the solution at iteration  $k+1$  of the iterative process is obtained by applying the first-order optimality condition<sup>5</sup> to the functional:

$$J_{OMR}(\mathbf{F}) = \|\mathbf{X} - \mathbf{H}\mathbf{F}\|_2^2 \cdot \sum_{r=1}^R \|\mathbf{F}_r\|_{q_r}^{q_r}. \quad (8)$$

In doing so, one obtains, after some calculations, the following explicit expression:

$$\widehat{\mathbf{F}}^{(k+1)} = \left( \mathbf{H}^H \mathbf{H} + \alpha^{(k+1)} \mathbf{W}^{(k+1)} \right)^{-1} \mathbf{H}^H \mathbf{X}, \quad (9)$$

---

<sup>4</sup>Such information can be roughly obtained from the analysis of the mechanical system.

<sup>5</sup>The first-order optimality condition consists in setting the gradient of the considered functional with respect to the sought quantity, here  $\mathbf{F}$ , to zero.

where the adaptive regularization parameter  $\alpha^{(k+1)}$  is written:

$$\alpha^{(k+1)} = \frac{\left\| \mathbf{X} - \mathbf{H}\widehat{\mathbf{F}}^{(k)} \right\|_2^2}{\sum_{r=1}^R \left\| \widehat{\mathbf{F}}_{\mathbf{r}}^{(k)} \right\|_{q_r}^{q_r}}, \quad (10)$$

while the global weighting matrix  $\mathbf{W}^{(k+1)}$  is defined such that:

$$\mathbf{W}^{(k+1)} = \text{diag} \left( \mathbf{W}_{\mathbf{1}}^{(k+1)}, \dots, \mathbf{W}_{\mathbf{R}}^{(k+1)} \right). \quad (11)$$

In the previous equation, each local weighting matrix  $\mathbf{W}_{\mathbf{r}}^{(k+1)}$  is a diagonal matrix, given by:

$$\mathbf{W}_{\mathbf{r}}^{(k+1)} = \text{diag} \left[ w_{r,1}^{(k+1)}, \dots, w_{r,i}^{(k+1)}, \dots, w_{r,N_r}^{(k+1)} \right] \quad (12)$$

with:

$$w_{r,i}^{(k+1)} = \frac{q_r}{2} \max \left( \epsilon_r, \left| f_{ri}^{(k)} \right| \right)^{q_r-2}, \quad (13)$$

where  $N_r$  is the number of identification points in the zone  $\mathbf{r}$ ,  $f_{ri}^{(k)}$  is the  $i^{\text{th}}$  component of the vector  $\widehat{\mathbf{F}}_{\mathbf{r}}^{(k)}$  and  $\epsilon_r$  is a small positive number avoiding infinite weights when  $\left| f_{ri}^{(k)} \right| \rightarrow 0$  and  $q_r < 2$ . Practically,  $\epsilon_r$  is chosen so that 5% of the values of  $\left| \widehat{\mathbf{F}}_{\mathbf{r}}^{(0)} \right|$  are less than or equal to  $\epsilon_r$  [13, 46].

### 3.2.2. Main iteration for the MPMR

For the MPMR, the solution at iteration  $k+1$  of the iterative process is obtained by applying the first-order optimality condition to the functional:

$$J_{MPMR}(\mathbf{F}) = \left\| \mathbf{X} - \mathbf{H}\mathbf{F} \right\|_2^2 \cdot \prod_{r=1}^R \left\| \mathbf{F}_{\mathbf{r}} \right\|_{q_r}^{q_r}. \quad (14)$$

In doing so, one obtains the following explicit expression:

$$\widehat{\mathbf{F}}^{(k+1)} = \left( \mathbf{H}^H \mathbf{H} + \mathbf{L}_{\mathbf{W}}^H \boldsymbol{\Lambda}^{(k+1)} \mathbf{L}_{\mathbf{W}} \right)^{-1} \mathbf{H}^H \mathbf{X}, \quad (15)$$

where  $\mathbf{L}_\mathbf{W} = \mathbf{W}^{(k+1)1/2}$  [see Eqs. (11) and (12) for the definition of  $\mathbf{W}^{(k+1)}$ ] and  $\mathbf{\Lambda}^{(k+1)}$  is the adaptive regularization matrix defined such that:

$$\mathbf{\Lambda}^{(k+1)} = \text{diag} \left( \alpha_1^{(k+1)} \mathbf{1}_1, \dots, \alpha_R^{(k+1)} \mathbf{1}_R \right) \text{ with } \alpha_r^{(k+1)} = \frac{\left\| \mathbf{X} - \mathbf{H}\widehat{\mathbf{F}}^{(k)} \right\|_2^2}{\left\| \mathbf{L}_r \widehat{\mathbf{F}}_r^{(k)} \right\|_{q_r}^{q_r}}, \quad (16)$$

where  $\mathbf{1}_r$  is the unit vector of dimension  $N_r$ .

### 3.3. Convergence monitoring - Stopping criterion

As any iterative procedure, the proposed algorithm must be stopped either after a certain stopping criterion is satisfied or after a certain number of iterations fixed by the user is reached. In the present paper, the convergence of the iterative process is monitored via the variation of relative error of the force vector between two successive iterations. Mathematically, the relative error  $\delta$  is defined such that:

$$\delta \left( \widehat{\mathbf{F}}^{(k-1)}, \widehat{\mathbf{F}}^{(k)} \right) = \frac{\left\| \widehat{\mathbf{F}}^{(k)} - \widehat{\mathbf{F}}^{(k-1)} \right\|_1}{\left\| \widehat{\mathbf{F}}^{(k-1)} \right\|_1}. \quad (17)$$

In such a case, the iterative process is classically stopped when  $\delta$  reaches some tolerance, set here to  $10^{-4}$ , which allows obtaining a fair compromise between the solution accuracy and the computational efficiency.

## 4. Numerical validation

The proposed numerical validation intends to assess the pertinence of the MPMR for identifying the excitation sources acting on a mechanical structure by comparing the results it provides with those stemming from the

OMR. More specifically, the overall performances of both formulation with respect to the measurement noise level, as well as the resolution algorithm implemented to solve the reconstruction problem will be carefully studied. The latter point aims at providing further insights regarding the importance of the definition of the resolution procedure used to solve the OMR and the MPMR. Consequently, this numerical validation allows focusing on the intrinsic behavior of the compared algorithms by avoiding any experimental bias (modeling error, geometrical uncertainties, location uncertainties of the measurement points, ...).

#### *4.1. Problem description*

In the present numerical validation, we are interested in the identification a harmonic point force of unit amplitude exciting, at 350 Hz<sup>6</sup>, a thin simply supported steel plate with dimensions 0.6 m  $\times$  0.4 m  $\times$  0.005 m as well as the related reaction forces. The coordinates of the point force, measured from the lower left corner of the plate, are  $(x_0, y_0) = (0.42 \text{ m}, 0.25 \text{ m})$ . The main interest of this test case is to exhibit two types of spatial distribution over the structure, namely a smooth distribution of the reaction forces at boundaries and a sparse distribution around the location of the point force. It results that this numerical validation is perfectly adapted to assess the pertinence of the proposed multi-parameter strategy.

To implement this numerical validation, the synthesized vibration field as well as the transfer functions matrix must be defined. The simulation of the

---

<sup>6</sup>This frequency has been chosen, because it lies outside the resonance frequencies of the plate.

experimental data is performed in two steps. First, the exact displacement field  $\mathbf{X}_{\text{exact}}$  is computed from a FE mesh of the plate made up with 187 shell elements, assuming that only bending motions are measurable. Then, a Gaussian white noise with a prescribed SNR is added to the exact data to simulate measurement errors, related to the transducers quality. Regarding now the definition of the transfer functions matrix  $\mathbf{H}$ , it has been chosen to compute it from the FE model of the plate with free boundary conditions, assuming, here again, that only bending motions are measured. Such an approach makes the identification of the point force excitation and the reaction forces at boundaries possible. From a theoretical standpoint, this is easily explained by recalling that the system considered for the reconstruction is, in that case, the plate without its supports. Consequently, the reaction forces induced by the supports to ensure the mechanical connection are then considered as external forces.

#### 4.2. Application

To numerically validate any force reconstruction strategy, it is first necessary to define the force vector  $\mathbf{F}_{\text{ref}}$  that could serve as a proper reference. This reference force vector is obtained from the transfer functions matrix  $\mathbf{H}$  and the exact displacement field  $\mathbf{X}_{\text{exact}}$  by applying the following relation:

$$\mathbf{F}_{\text{ref}} = \mathbf{H}^{-1}\mathbf{X}_{\text{exact}}. \quad (18)$$

As shown in Fig. 1, the reference force vector exhibits smooth reaction forces at boundaries of the plate as well as a unit point force  $F_0$  at  $(x_0, y_0) = (0.42 \text{ m}, 0.25 \text{ m})$  as expected from the description of the test case. This consequently suggests the definition of two identification regions in order to

apply the OMR and the MPMR: (i) a central region associated to the norm parameter  $q_1$  and including the point force only and (ii) a region associated to the norm parameter  $q_2$  and corresponding to the boundaries of the plate [see Fig. 2]. Regarding the choice of norm parameters  $q_1$  and  $q_2$ , their values are set in order to reflect one's prior knowledge of the sources to identify in each region. In the present case, the value of the norm parameter  $q_1$  has to enforce the sparsity of the solution vector in this region, i.e. by setting  $q_1 \leq 1$  [47, 48]. On the contrary, the value of the norm parameter  $q_2$  must be chosen in order to promote distributed sources, which is generally done by defining  $q_2 = 2$  [7]. From what precedes and from our experience of this kind of problems, it has been chosen to set  $(q_1, q_2) = (0.5, 2)$ .

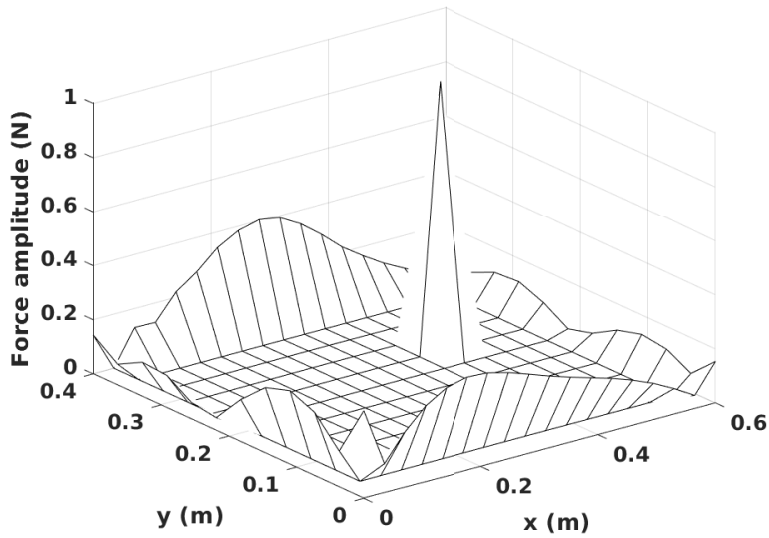


Figure 1: Reference force vector  $\mathbf{F}_{\text{ref}}$  at 350 Hz

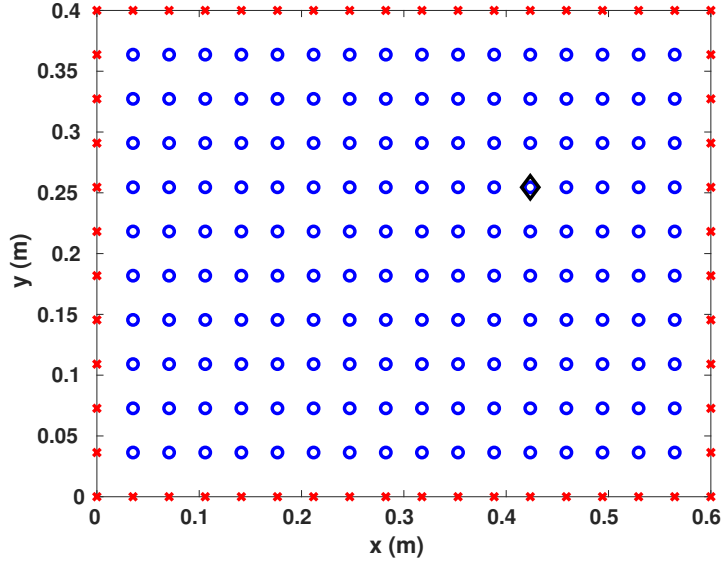


Figure 2: Definition of the identification regions - ( $\circ$ ) region 1 (Point force), ( $\times$ ) region 2 (Reaction forces) and ( $\diamond$ ) location of the point force

#### 4.3. Influence of the measurement noise level

One of the main question for any inverse method is the robustness of the results identified with respect to the noise corrupting the data. To obtain further insights regarding this important question, let us first consider the identification of the excitation field from a vibration field having a SNR equal to 35 dB. For this relatively high SNR, the excitation fields reconstructed from the OMR-IR and MPMR-IR algorithms are presented in Fig. 3. The visual inspection of this figure suggests that the reconstructed excitation field is in good agreement with the reference one, whatever the formulation and the associated resolution algorithm considered.

To confirm this qualitative observation, the accuracy of the reconstructed

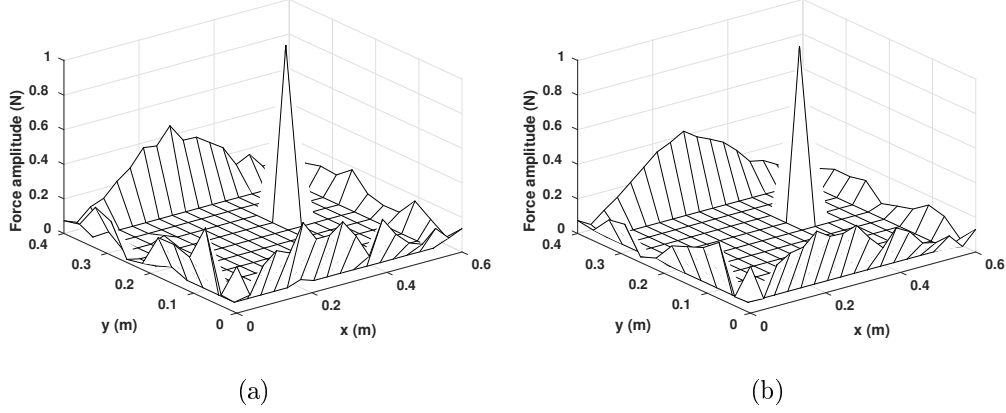


Figure 3: Reconstructed excitation field at 350 HZ from vibration data having a SNR equal to 35 dB – (a) OMR-IR algorithm and (b) MPMR-IR algorithm –  $(q_1, q_2) = (0.5, 2)$

solutions are quantified from the global relative error (GRE), the relative error on the identification of the reaction forces (RERF) and the peak error (PE). Formally, the global relative error is a global indicator of the reconstruction quality, defined by the relation:

$$\text{GRE} = \frac{\|\widehat{\mathbf{F}} - \mathbf{F}_{\text{ref}}\|_1}{\|\mathbf{F}_{\text{ref}}\|_1}. \quad (19)$$

In the same vein, the relative error on the reaction forces is an indicator of the reconstruction quality of the reaction forces. Its mathematical definition is similar to the relative error, since:

$$\text{RERF} = \frac{\|\widehat{\mathbf{F}}^{(2)} - \mathbf{F}_{\text{ref}}^{(2)}\|_1}{\|\mathbf{F}_{\text{ref}}^{(2)}\|_1} \quad (20)$$

where  $\widehat{\mathbf{F}}^{(2)}$  is the force vector identified in region 2, while  $\mathbf{F}_{\text{ref}}^{(2)}$  is the reference force vector in the same region.

Contrary to the previous indicators, the peak error is a local indicator describing the reconstruction quality of the point force amplitude. Mathematically, it is defined such that:

$$\text{PE} = \frac{\widehat{F}_p - F_p^{\text{ref}}}{F_p^{\text{ref}}}, \quad (21)$$

where  $F_p^{\text{ref}}$  is the point force amplitude associated to the reference force vector  $\mathbf{F}_{\text{ref}}$ , while  $\widehat{F}_p$  is the point force amplitude associated to the identified solution  $\widehat{\mathbf{F}}$  at point  $(x_0, y_0)$ .

The results gathered in Table 1 allows going further in the analysis of the overall performances of the proposed regularization strategies and the related resolution algorithms. In particular, it is shown that the reconstruction of the point force excitation is properly carried out by both approaches. It is interesting to note that the OMR-IR algorithm leads to a slight overestimation of the point force amplitude, while the MPMR-IR algorithm tends to slightly underestimate it. However, the analysis of the GRE and the RERF indicators points out that the reconstruction of the reaction forces is not as good as expected, especially for the OMR-IR algorithm. In terms of computational efficiency, it should be noticed that the MPMR-IR algorithm requires half as much iterations as the OMR-IR algorithm to reach the convergence. Finally, it may be noticed that the converged value of the adaptive parameters for the MPMR-IR algorithm is about one order of magnitude greater than the adaptive regularization parameter estimated from the OMR-IR algorithm.

Perhaps more interesting is the behavior of the considered resolution algorithms when the SNR gets lower. All the results obtained for SNR values ranging from 30 dB to 5 dB are respectively given in Table 2 and Fig. 4

Table 1: Performances of the OMR-IR and MPMR-IR algorithms for high-SNR data (SNR = 35 dB) –  $N_{it}$ : Number of iterations of the algorithm,  $\alpha_i$ : Converged value of the adaptive regularization parameter in the region  $i$

	<b>Resolution algorithm</b>	
	<b>OMR-IR</b>	<b>MPMR-IR</b>
PE (%)	0.6	-0.01
RERF (%)	35.75	19.65
GRE (%)	34.83	18.67
$\alpha_1$	$9.32 \times 10^{-16}$	$2.25 \times 10^{-15}$
$\alpha_2$		$4.15 \times 10^{-15}$
$N_{it}$	26	12

for the OMR-IR strategy and in Table 3 and Fig. 5 for the MPMR-IR approach. A careful analysis of the results of the OMR-IR algorithm indicates that the reconstruction is rather constant in terms of solution accuracy and number of iterations from high (30 dB) to low (10 dB) SNR values. However, in case of extremely noisy vibration data, the point force location is not properly identified [see PE in Table 2 and Fig. 4d], while the estimation of the reaction forces is similar to that obtained for higher SNR values. A closer look at Fig. 4d actually shows that the identified point force is located at  $(\hat{x}_0, \hat{y}_0) = (0.46 \text{ m}, 0.25 \text{ m})$  with an amplitude of 0.81 N instead of  $(x_0, y_0) = (0.42 \text{ m}, 0.25 \text{ m})$  and 1 N for the reference excitation. All things considered, the results obtained for such a low SNR is quite satisfying, since the PE, computed from the amplitude obtained at the identified point force location, is equal to -20%, while the location error is less than 10% (here 4

cm along the length of the plate). It should be noted that the previous result can be improved in terms relative errors and location error by selecting  $\alpha^{(0)}$  from standard automatic selection procedures. For the sake of completeness, the corresponding results are presented in [Appendix A](#).

Table 2: Performances of the OMR-IR algorithm for with respect to the noise corrupting the data

	SNR (dB)					
	30	25	20	15	10	5
PE (%)	0.88	1.48	2.11	2.45	0.24	-99
RERF (%)	36.35	33.98	33.32	31.96	32.22	35.37
GRE (%)	33.98	31.97	31.97	31.16	32.33	53.51
$\alpha$	$3.24 \times 10^{-15}$	$1.09 \times 10^{-14}$	$3.33 \times 10^{-14}$	$1.09 \times 10^{-13}$	$3.28 \times 10^{-13}$	$8.44 \times 10^{-13}$
$N_{it}$	16	13	13	13	15	17

Contrary to what it is observed for the OMR-IR algorithm, Table 3 and Fig. 5 show that the MPMR-IR algorithm behaves rather differently as the SNR gets lower. Indeed, one can observed that satisfying reconstruction are obtained for high and moderate SNR values, i.e. above 20 dB. Between 20 dB and 15 dB, the amplitude of the identified point force decreases significantly. Below this SNR value, the MPMR-IR algorithm converges to the zero vector, since the converged values of  $\alpha_1$  and  $\alpha_2$  tends to infinity. It should be noted here that selecting  $\alpha^{(0)}$  from standard automatic selection procedures does not improve the quality of the identified solutions.

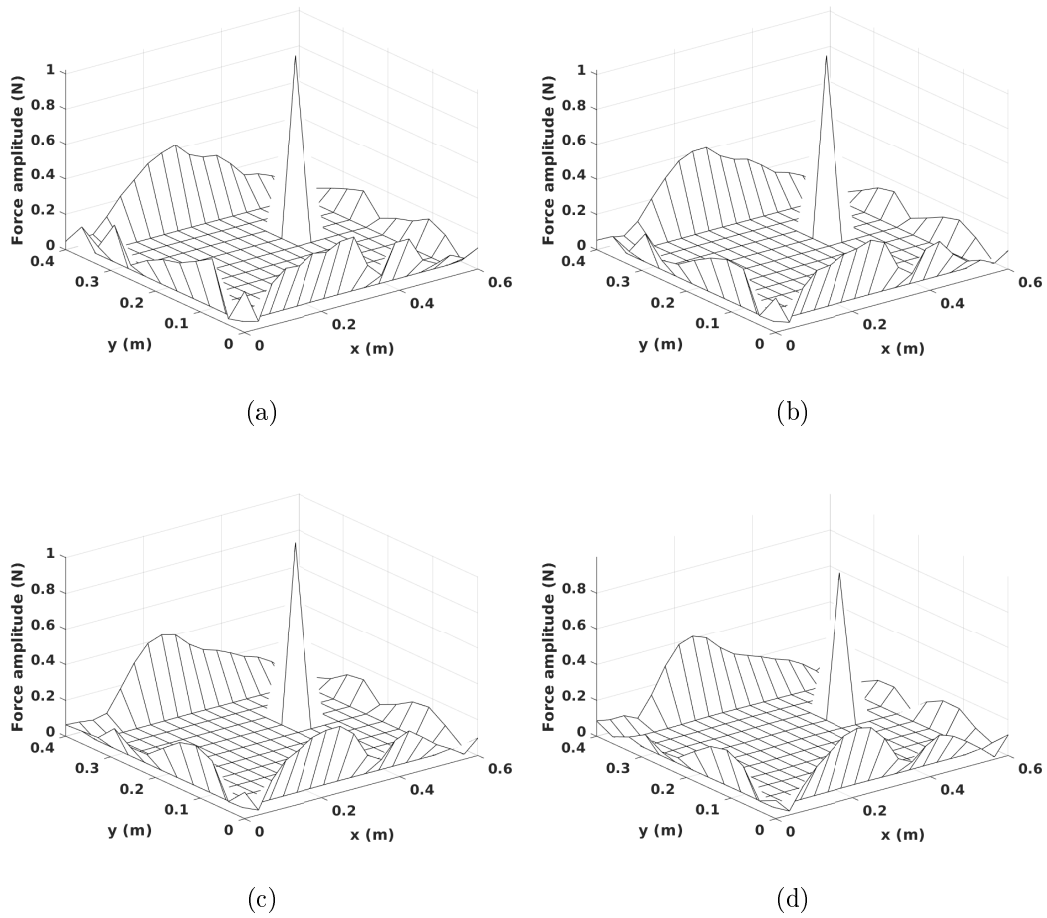


Figure 4: Reconstructed excitation field at 350 HZ from OMR-IR for different SNR values  
 – (a) 20 dB, (b) 15 dB, (c) 10 dB and (d) 5 dB –  $(q_1, q_2) = (0.5, 2)$

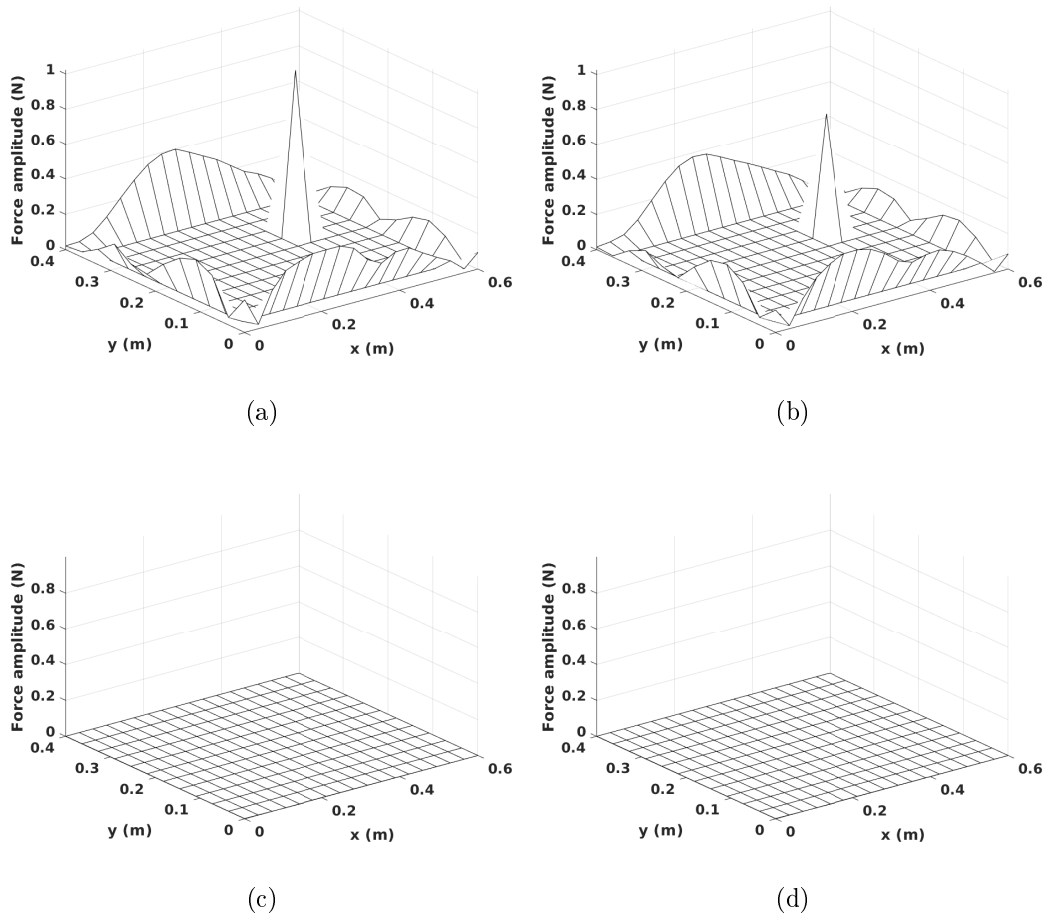


Figure 5: Reconstructed excitation field at 350 HZ from MPMR-IR for different SNR values – (a) 20 dB, (b) 15 dB, (c) 10 dB and (d) 5 dB –  $(q_1, q_2) = (0.5, 2)$

Table 3: Performances of the MPMR-IR algorithm for with respect to the noise corrupting the data

	SNR (dB)					
	30	25	20	15	10	5
PE (%)	-0.18	-1.56	-6.25	-30.68	-100	-100
RERF (%)	19.18	18.73	18.84	20.31	100	100
GRE (%)	18.51	18.36	18.83	22.41	100	100
$\alpha_1$	$8.40 \times 10^{-15}$	$3.14 \times 10^{-14}$	$8.85 \times 10^{-14}$	$3.12 \times 10^{-13}$	$+\infty$	$+\infty$
$\alpha_2$	$1.37 \times 10^{-14}$	$4.57 \times 10^{-14}$	$1.55 \times 10^{-13}$	$6.51 \times 10^{-13}$	$+\infty$	$+\infty$
$N_{it}$	12	12	13	23	25	19

In the light of these results, it seems that in case low-SNR data the MPMR-IR algorithm has too many degrees of freedom to ensure a proper estimation of both the point force excitation and the reaction forces. In this respect, the greater flexibility in the tuning of the adaptive regularization parameters offered by the MPMR is not as beneficial as expected at first sight.

#### 4.4. Influence of the resolution algorithm

Practically, several algorithms can be implemented to solve the OMR and the MPMR formulations. One of the classical way to solve these regularization strategies is the Iteratively Least-Squares algorithm [49, 50]. To provide further insights regarding the importance of the definition of the resolution procedure used to solve the OMR and the MPMR, this section aims at analyzing the results obtained from an IRLS implementation for

both the formulations. These resolution algorithm are respectively referred to as OMR-IRLS and MPMR-IRLS in the rest of the paper. For the sake of brevity, OMR-IRLS and MPMR-IRLS algorithms are described in [Appendix B](#). It should be mentioned here that the OMR-IRLS is the algorithm we have implemented in Ref. [15].

The results obtained from the OMR-IRLS algorithm and presented in Table 4 show that for high and moderate SNR values, i.e. above 20 dB, the algorithm behaves relatively well, since consistent reconstructions are obtained. As observed for the MPMR-IR algorithm, between 20 dB and 15 dB, the amplitude of the identified point force is greatly underestimated (see Fig. 6). Even worse, for very low SNR values, the OMR-IRLS algorithm returns a NaN vector, meaning that the value of the adaptive regularization parameter becomes undetermined along the iterations.

Table 4: Performances of the OMR-IRLS algorithm for with respect to the noise corrupting the data

	SNR (dB)					
	30	25	20	15	10	5
PE (%)	-0.25	-1.50	-7.91	-99	NaN	NaN
RERF (%)	22.68	21.44	20.85	26.25	NaN	NaN
GRE (%)	21.67	20.79	20.77	33.81	NaN	NaN
$\alpha$	$9.16 \times 10^{-15}$	$3.10 \times 10^{-14}$	$1.06 \times 10^{-13}$	$1.65 \times 10^{-12}$	NaN	NaN
$N_{it}$	14	13	14	25	24	17

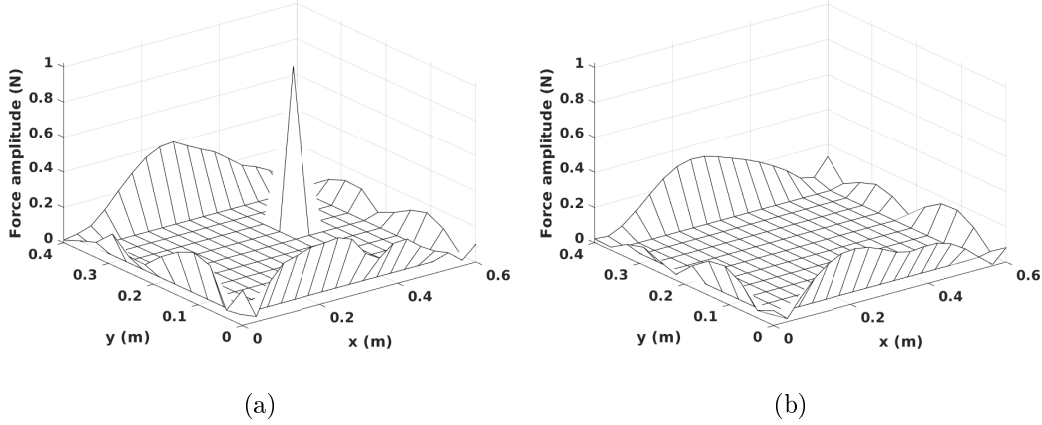


Figure 6: Reconstructed excitation field at 350 HZ from OMR-IRLS for different SNR values – (a) 20 dB and (b) 15 dB –  $(q_1, q_2) = (0.5, 2)$  – For SNR values equal to 10 dB and 5 dB the OMR-IRLS algorithm returns a NaN vector

In the case of the MPMR-IRLS algorithm, consistent results are obtained up to a SNR equal to 25 dB. Below this value, unreliable results are obtained, since one or both adaptive regularization parameters tends to infinity (see Table 5 and Fig. 7). As a side note, It is worth noting that selecting  $\alpha^{(0)}$  from standard automatic selection procedures has no impact on the solutions finally identified from the OMR-IRLS and MPMR-IRLS algorithms.

This study clearly points out that the choice of the resolution algorithm is not neutral in terms of solution accuracy. In the present application, it appears that the OMR and the MPMR performs equally well for high-SNR data, whatever the resolution algorithm used to solve them. However, OMR-IR and MPMR-IR algorithms are more robust than their IRLS counterpart with respect to the measurement noise level. Indeed, in case of low-SNR data,

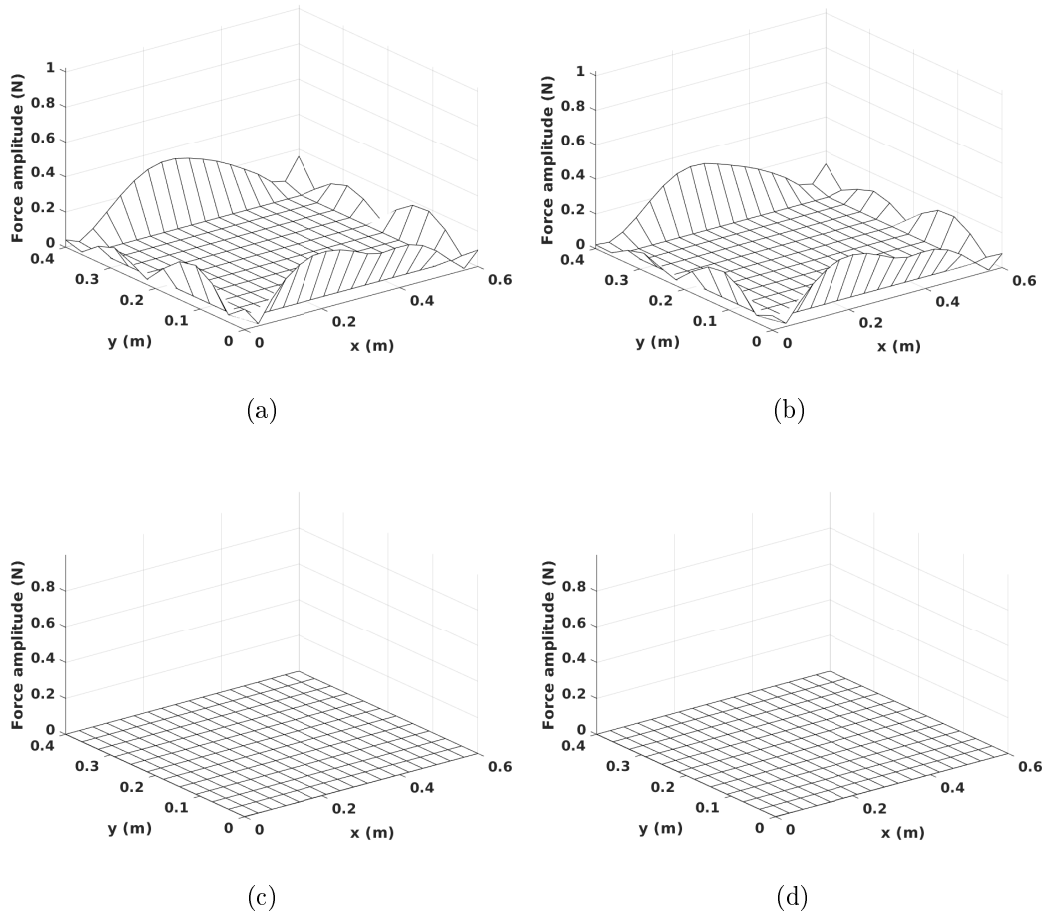


Figure 7: Reconstructed excitation field at 350 HZ from MPMR-IRLS for different SNR values – (a) 20 dB, (b) 15 dB, (c) 10 dB and (d) 5 dB -  $(q_1, q_2) = (0.5, 2)$

Table 5: Performances of the MPMR-IRLS algorithm for with respect to the noise corrupting the data

	SNR (dB)					
	30	25	20	15	10	5
PE (%)	-2.98	-12.49	-100	-100	-100	-100
RERF (%)	18.24	17.49	22.39	26.55	100	100
GRE (%)	18.05	18.20	30.31	34.04	100	100
$\alpha_1$	$3.79 \times 10^{-14}$	$1.42 \times 10^{-13}$	$+\infty$	$+\infty$	$+\infty$	$+\infty$
$\alpha_2$	$1.54 \times 10^{-14}$	$5.57 \times 10^{-14}$	$8.71 \times 10^{-13}$	$1.73 \times 10^{-12}$	$+\infty$	$+\infty$
$N_{it}$	12	17	18	18	18	15

the OMR associated to the OMR-IR algorithm is the better option, even if the MPMR solved from the MPMR-IR algorithm remains, to a certain extent, a viable alternative.

## 5. Conclusion

This paper has been focused on the applicability of a multi-parameter multiplicative regularization (MPMR) for solving force reconstruction problems, compared to a more classical single parameter approach recently published by the authors, called ordinary multiplicative regularization (OMR). From a numerical standpoint, each formulation is solved from an original Iteratively Reweighted (IR) algorithm obtained from the direct application of the first-order optimality condition. In this contribution, the resulting resolution procedures are named OMR-IR and MPMR-IR algorithms respectively. To assess the ability of each formulation in properly reconstructing excita-

tion sources acting on a mechanical structure, a numerical experiment has been conducted. In particular, it has been demonstrated that OMR-IR and MPMR-IR algorithms are more robust than the corresponding IRLS versions with respect to the measurement noise level. Consequently, regarding the initial motivation of this work, both the OMR and the MPMR are viable alternatives, provided that a suitable resolution algorithm is implemented. For high and moderate measurement noise levels, the MPMR-IR algorithm provides more accurate results than the OMR-IR algorithm. In case of very noisy data, however, only the OMR-IR algorithm, allows obtaining consistent reconstruction. To sum up, it may be concluded that the MPMR formulation, associated to the IR algorithm introduced in this paper, is interesting if the measurement vibration data are rather clean. From a general standpoint, the OMR-IR strategy is however the safer option if the measurement noise level is unknown, because it provides a good compromise in terms of solution accuracy for a large range of measurement noise level.

### **Appendix A. Influence of the selection of the initial adaptive regularization parameter for OMR-IR algorithm and low SNR value**

In case of extremely noisy vibration data, the choice of the initial adaptive regularization parameter  $\alpha^{(0)}$  is crucial. To demonstrate this statement, Table A.1 and Fig. A.1 gather the results obtained by applying of the OMR-IR algorithm from a displacement field having a SNR of 5 dB and selecting  $\alpha^{(0)}$  from the L-curve principle (LC) [44], the Generalized Cross Validation (GCV) [42] and the Bayesian Estimator (BE) [45]. Presented results high-

light the influence of the procedure used to initialize  $\alpha^{(0)}$  in case of very low SNR data. Indeed, when the parameter is selected from the GCV or the BE, reasonable reconstructions are obtained considering the noise level applied to the displacement data. On the contrary, when the parameter  $\alpha^{(0)}$  is picked by the L-curve, the OMR-IR algorithm is unable to properly identify the point force, since in the corresponding region the solution vector is the zero vector. The latter result can be explained by comparing for each selection procedure the values  $\alpha^{(0)}$  and  $\alpha$  (converged value of the adaptive regularization parameter) given in Table A.1. While  $\alpha^{(0)}$  is about one order of magnitude less than  $\alpha$  for the GCV and the BE, it is actually greater than  $\alpha$  for the L-curve. This implies that the initial solution is probably too smooth to expect the convergence of the OMR-IR algorithm to a meaningful identified solution.

Table A.1: Performances of the OMR-IR for low SNR data (SNR = 5 dB) with respect to the selection procedure used to set  $\alpha^{(0)}$

	Selection procedure		
	LC	GCV	BE
PE (%)	-99	-21.28	-26.30
RERF (%)	33.85	31.34	31.02
GRE (%)	40.87	32.08	31.96
$\alpha^{(0)}$	$2.33 \times 10^{-12}$	$6.40 \times 10^{-13}$	$7.08 \times 10^{-13}$
$\alpha$	$2.21 \times 10^{-12}$	$1.40 \times 10^{-12}$	$1.57 \times 10^{-12}$
$N_{it}$	17	22	28

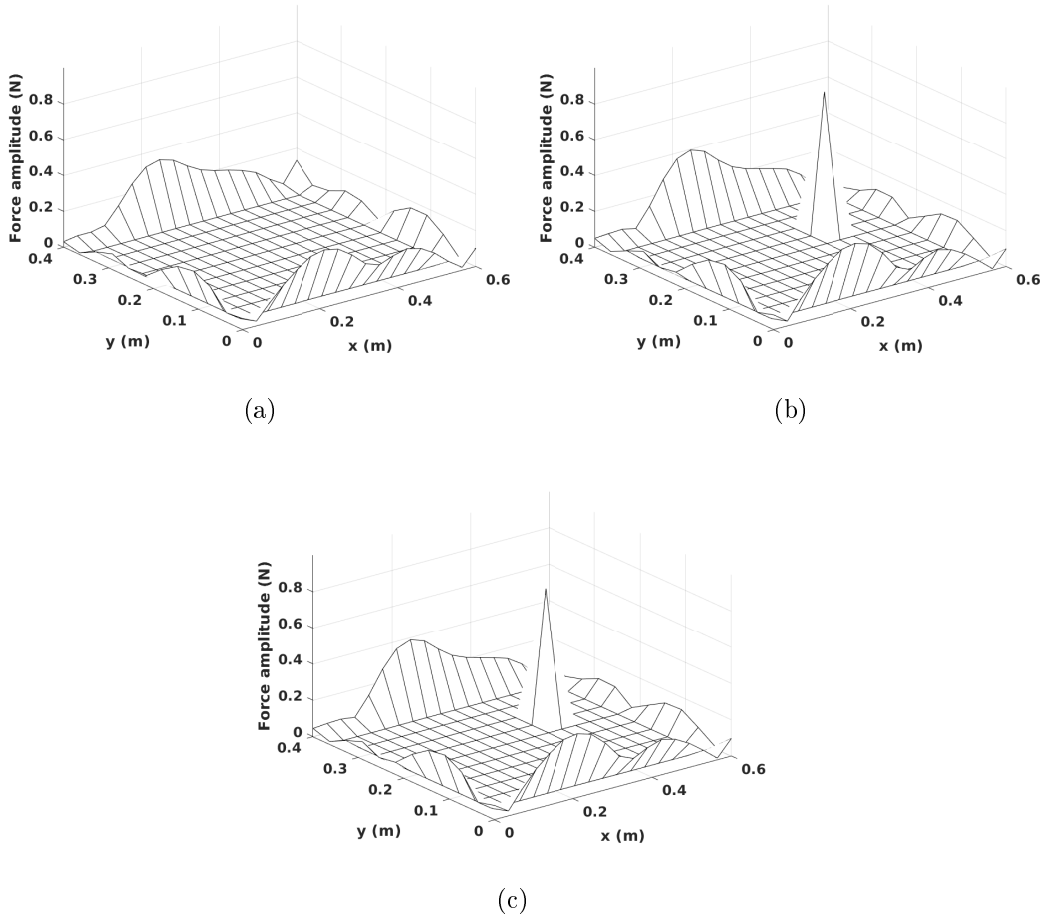


Figure A.1: Reconstructed excitation field at 350 HZ from OMR-IR from vibration data having a SNR equal to 35 dB after applying different selection procedure to set the value of  $\alpha^{(0)}$  – (a) L-curve principle, (b) Generalized Cross Validation and (c) Bayesian Estimator –  $(q_1, q_2) = (0.5, 2)$

## Appendix B. Description of the OMR-IRLS and MPMR-IRLS algorithms

This appendix aims at presenting the necessary changes in the OMR-IR and MPMR-IR algorithms to obtain the corresponding OMR-IRLS and MPMR-IRLS algorithms. From a theoretical standpoint, the core idea of the OMR-IRLS and the MPMR-IRLS algorithms is to recast at each iteration of the iterative process the  $\ell_{q_r}$ -norm into a weighted  $\ell_2$ -norm. In other words, the sought excitation vector at iteration  $k + 1$  is solution of:

$$\widehat{\mathbf{F}}^{(k+1)} = \underset{\mathbf{F} \setminus \{0\}}{\operatorname{argmin}} \|\mathbf{X} - \mathbf{H}\mathbf{F}\|_2^2 \cdot \sum_{r=1}^R \|\mathbf{W}_r^{(k+1)1/2} \mathbf{F}_r\|_2^2, \quad (\text{B.1})$$

for the OMR-IRLS algorithm, while for the MPMR-IRLS algorithm, it is the solution of:

$$\widehat{\mathbf{F}}^{(k+1)} = \underset{\mathbf{F} \setminus \{0\}}{\operatorname{argmin}} \|\mathbf{X} - \mathbf{H}\mathbf{F}\|_2^2 \cdot \prod_{r=1}^R \|\mathbf{W}_r^{(k+1)1/2} \mathbf{F}_r\|_2^2, \quad (\text{B.2})$$

### Appendix B.1. OMR-IRLS algorithm

To obtain the OMR-IRLS algorithm, one just has to modify the OMR-IR algorithm by changing the definition of the coefficients of the local weighting matrix and the expression of the adaptive regularization parameter, given by Eqs. (10) and (13). For the OMR-IRLS, one has:

$$\alpha^{(k+1)} = \frac{\|\mathbf{X} - \mathbf{H}\widehat{\mathbf{F}}^{(k)}\|_2^2}{\|\mathbf{W}^{(k+1)1/2} \widehat{\mathbf{F}}^{(k)}\|_2^2}, \quad \text{and} \quad w_{r,i}^{(k+1)} = \max\left(\epsilon_r, \left|f_{ri}^{(k)}\right|\right)^{q_r-2}. \quad (\text{B.3})$$

### Appendix B.2. MPMR-IRLS algorithm

To obtain the MPMR-IRLS algorithm, one just has to modify the MPMR-IR algorithm by changing the definition of the local adaptive regularization

parameters, given by Eq. (16). For the MPMR-IRLS algorithm, one has:

$$\alpha_r^{(k+1)} = \frac{\left\| \mathbf{X} - \mathbf{H}\hat{\mathbf{F}}^{(k)} \right\|_2^2}{\left\| \mathbf{W}_r^{(k+1)1/2} \hat{\mathbf{F}}_r^{(k)} \right\|_2^2}, \quad (\text{B.4})$$

where the coefficients of the local weighting matrices are defined in Eq. (B.3).

## References

- [1] E. Jacquelin, A. Bennani, P. Hamelin, Force reconstruction: analysis and regularization of a deconvolution, *J. Sound Vib.* 265 (2003) 81–107.
- [2] Q. Leclere, C. Pezerat, B. Laulagnet, L. Polac, Indirect measurement of main bearing loads in an operating diesel engine, *J. Sound Vib.* 286 (1-2) (2005) 341–361.
- [3] Y. Liu, W. Steve Shepard Jr., Reducing the impact of measurement errors when reconstructing dynamic forces, *J. Vib. Acoust.* 128 (2006) 586–593.
- [4] A. N. Thite, D. J. Thompson, The quantification of structure-borne transmission paths by inverse methods. Part 2 : Use of regularization techniques, *J. Sound Vib.* 264 (2) (2003) 433–451.
- [5] Y.-M. Mao, X.-L. Guo, Y. Zhao, Experimental study of hammer impact identification on a steel cantilever beam, *Exp. Tech.* 34 (3) (2010) 82–85.
- [6] E. Turco, Tools for the numerical solution of inverse problems in structural mechanics: review and research perspectives, *Eur. J. Environ. Civ. Eng.* 21 (5) (2017) 509–554.

- [7] S. Boyd, L. Vandenberghe, *Convex optimization*, Cambridge University Press, New York, 2004.
- [8] C. Renzi, C. C. Pezerat, J.-L. Guyader, Vibration sources identification using vibratory measurements injected in a local finite element model, in: *Proc. ISMA 2010*, Luven, Belgium, 2010.
- [9] D. Ginsberg, C.-P. Fritzen, New approach for impact detection by finding sparse solution, in: *Proc. ISMA 2014 - Int. Conf. Noise Vib. Eng. USD 2014 - Int. Conf. Uncertain. Struct. Dyn.*, Leuven, Belgium, 2014, pp. 2043–2056.
- [10] B. Qiao, X. Zhang, C. Wang, H. Zhang, X. Chen, Sparse regularization for force identification using dictionaries, *J. Sound Vib.* 368 (2016) 71–86.
- [11] B. Qiao, X. Zhang, J. Gao, X. Chen, Impact-force sparse reconstruction from highly incomplete and inaccurate measurements, *J. Sound Vib.* 376 (2016) 72–94.
- [12] C.-D. Pan, L. Yu, H.-L. Liu, Z.-P., W.-F. Luo, Moving force identification based on redundant concatenated dictionary and weighted  $\ell_1$ -norm regularization, *Mech. Syst. Signal Process.* 98 (2018) 32–49.
- [13] M. Aucejo, Structural source identification using a generalized Tikhonov regularization, *J. Sound Vib.* 333 (22) (2014) 5693–5707.
- [14] M. Aucejo, O. D. Smet, Bayesian source identification using local priors, *Mech. Syst. Signal Process.* 66-67 (2016) 120–136.

- [15] M. Aucejo, O. D. Smet, A multiplicative regularization for force reconstruction, *Mech. Syst. Signal Process.* 85 (2017) 730–745.
- [16] P. M. van den Berg, A. Abubakar, J. T. Fokkema, Multiplicative regularization for contrast profile inversion, *Radio Sci.* 38 (2003) 8022–8031.
- [17] D. H. Brooks, G. F. Ahmad, R. S. MacLeod, G. M. Maratos, Inverse electrocardiography by simultaneous imposition of multiple constraints, *IEEE Trans. Biomed. Eng.* 46 (1) (1999) 3–18.
- [18] M. Belge, L. Kilmer, E. Miller, Wavelet domain image restoration with adaptive edge-preserving regularization, *IEEE Trans. Image Process.* 9 (4) (2000) 597–608.
- [19] H. Zou, T. Hastie, Regularization and variable selection via the elastic net, *J. R. Stat. Soc. B* 67 (2) (2005) 301–320.
- [20] Y. Lu, L. Shen, Y. Xu, Multi-parameter regularization methods for high-resolution image reconstruction with displacement errors, *IEEE Trans. Circuits Syst. I Regul. Pap.* 54 (8) (2007) 1788–1799.
- [21] W. Wang, S. Lu, H. Mao, J. Cheng, Multi-parameter Tikhonov regularization with the  $\ell_0$  sparsity constraint, *Inverse Probl.* 29 (2013) 065018 – 18 pp.
- [22] Q. Fan, D. Jiang, Y. Jiao, A multi-parameter regularization model for image restoration, *Signal Processing* 114 (2015) 131–142.
- [23] A. Deiveegan, Two-parameter regularization method for determining the heat source, *Glob. J. Pure Appl. Math.* 13 (8) (2017) 3937–3950.

- [24] S. Li, Z. Peng, Seismic acoustic impedance inversion with multi-parameter regularization, *J. Geophys. Eng.* 14 (2017) 520–532.
- [25] M. Belge, M. E. Kilmer, E. Miller, Efficient determination of multiple regularization parameter in a generalized L-curve framework, *Inverse Probl.* 18 (2002) 1161–1183.
- [26] C. Brezinski, M. Redivo-Zaglia, G. Rodriguez, S. Seatzu, Multi-parameter regularization techniques for ill-conditioned linear systems, *Numer. Math.* 94 (2003) 203–228.
- [27] K. Ito, B. Jin, T. Takeuchi, Multi-parameter Tikhonov regularization, *Methods Appl. Anal.* 18 (1) (2011) 31–46.
- [28] Z. Wang, Multi-parameter Tikhonov regularization and model function approach to the damped Morozov principle for choosing regularization, *J. Comput. Appl. Math.* 236 (2012) 1815–1832.
- [29] F. S. V. Bazan, S. Borges, J. B. Francisco, On a generalization of Regin-ska’s parameter choice rule and its numerical realization in large-scale multiple-parameter Tikhonov regularization, *Appl. Math. Comput.* 219 (2012) 2100–2113.
- [30] M. Green, Statistics of Images, the TV Algorithm of Rudin-Osher-Fatemi for Image Denoising and an Improved Denoising Algorithm, Tech. rep., UCLA (2002).
- [31] M. Nikolova, A variational approach to remove outliers and impulse noise, *J. Math. Imaging Vis.* 20 (1-2) (2004) 99–120.

- [32] T. Le, R. Chartrand, T. J. Asaki, A variational approach to reconstructing images corrupted by Poisson noise, *J. Math. Imaging Vis.* 27 (2007) 257–263.
- [33] A. Chambolle, Total Variation Minimization and a Class of Binary MRF Models, *Lect. Notes Comput. Sci.* 3757/2005 (2005) 136–152.
- [34] R. Tibshirani, Regression shrinkage and selection via the Lasso, *J. R. Stat. Soc. Ser. B* 58 (1) (1996) 267–288.
- [35] M. Hintermuller, T. Wu, Nonconvex  $TV^q$ -models in image restoration: Analysis and a trust-region regularization based superlinearly convergent solver., Tech. rep., Institute of Mathematics and Scientific Computing, University of Graz (2011).
- [36] J. Antoni, A Bayesian approach to sound source reconstruction: Optimal basis, regularization, and focusing, *J. Acoust. Soc. Am.* 131 (4) (2012) 2873–2890.
- [37] C. Faure, F. Ablitzer, J. Antoni, C. Pezerat, Empirical and fully Bayesian approaches for the identification of vibration sources from transverse displacement measurements, *Mech. Syst. Signal Process.* 94 (2017) 180–201.
- [38] M. Aucejo, O. D. Smet, On a full Bayesian inference for force reconstruction problems, *Mech. Syst. Signal Process.* 104 (2018) 36–59.
- [39] M. Aucejo, O. D. Smet, J. F. Deü, On a space-time regularization for force reconstruction problems, *Mech. Syst. Signal Process.* 118 (2019) 549–567.

- [40] M. Aucejo, O. D. Smet, On a general Iteratively Reweighted algorithm for solving force reconstruction problems, *J. Sound Vib.* 458 (2019) 376–388.
- [41] P. C. Hansen, Regularization tools: A matlab package for analysis and solution of discrete ill-posed problems, *Numer. algorithms* 6 (1994) 1–35.
- [42] G. H. Golub, M. Heath, G. Wahba, Generalized cross-validation as a method for choosing a good ridge parameter, *Technometrics* 21 (2) (1979) 215–223.
- [43] O. Scherzer, The use of Morozov’s discrepancy principle for Tikhonov regularization for solving nonlinear ill-posed problems, *Computing* 51 (1993) 45–60.
- [44] P. C. Hansen, Rank-Deficient and Discrete Ill-Posed Problems: Numerical Aspects of Linear Inversion, SIAM, Philadelphia, 1998.
- [45] A. Pereira, J. Antoni, Q. Leclere, Empirical Bayesian regularization of the inverse acoustic problem, *Appl. Acoust.* 97 (2015) 11–29.
- [46] P. Rodriguez, B. Wohlberg, Efficient Minimization Method for a Generalized Total Variation Functional, *IEEE Trans. Image Process.* 18 (2) (2009) 322–332.
- [47] R. Chartrand, V. Stavena, Nonconvex regularization for image segmentation, in: *Proc. Int. Conf. Image Process. Comput. Vis. Pattern Recognit.* 2007, Las Vegas, USA, 2007.

- [48] M. Nikolova, M. K. Ng, S. Zhang, W.-K. Ching, Efficient reconstruction of piecewise constant images using nonsmooth nonconvex minimization, *SIAM J. Imaging Sci.* 1 (1) (2008) 2–25.
- [49] P. J. Green, Iteratively Reweighted Least Squares for Maximum Likelihood Estimation, and some Robust and Resistant Alternatives, *J. R. Stat. Soc. Ser. B* 46 (2) (1984) 149–192.
- [50] P. Rodriguez, B. Wohlberg, An Iteratively Weighted Norm Algorithm for Total Variation Regularization, in: *Proc. 2006 Asilomar Conf. Signals, Syst. Comput.*, Pacific Grove, USA, 2006.